Editors' Suggestion

Raman signatures of the strong intramolecular and intermolecular charge oscillations in bis(ethylenedithio)-tetrathiafulvalene (BEDT-TTF) κ-phase salts

A. Girlando*
Molecular Materials Group (MoMaG), 43124 Parma, Italy

(Received 8 May 2024; accepted 13 June 2024; published 1 July 2024)

First-principle calculations of the Raman intensities of a $(BEDT\text{-}TTF)_2^+$ centrosymmetric dimer lead to a full reconsideration of the assignment of the three C=C stretching phonons in κ-phase BEDT-TTF salts. In contrast with previous interpretation, it is found that the presence of the out-of-phase coupling of the antisymmetric external C=C stretching mode has also to be taken into account. This mode, infrared-active for a single BEDT-TTF molecule, implies a strong intramolecular charge oscillation along BEDT-TTF long molecular axis. In the consequent reassignment of the C=C spectral region, a very broad band appearing in the cross polarized Raman spectra is interpreted as due to *inter*dimer electron-molecular vibration (e-mv) coupling, to be contrasted with the well-known intradimer e-mv coupling that induces very strong infrared absorptions. Analysis of the data in terms of a properly developed e-mv scheme yields an evaluation of the Hubbard parameters relevant to the so-called effective dimer model often used to interpret the physical properties of κ-BEDT-TTF salts. Finally, the Raman spectra of an asymmetric $(BEDT\text{-}TTF)^{+0.6}(BEDT\text{-}TTF)^{+0.4}$ dimer have been calculated in order to interpret the Raman spectra of the intriguing charge-ordered (CO), ferroelectric phase of κ-$(BEDT\text{-}TTF)_2Hg(SCN)_2Cl$. It turns out that in the asymmetric dimer the strong intradimer the e-mv induced infrared C=C stretching absorption should appear with huge intensity also in Raman. The absence of such band in the spectra of κ-$(BEDT\text{-}TTF)_2Hg(SCN)_2Cl$ ferroelectric phase points to an alternative CO pattern with respect to the one generally accepted so far.

DOI: 10.1103/PhysRevB.110.035101

I. INTRODUCTION

The salts of bis(ethylenedithio)-tetrathiafulvalene (BEDT-TTF, ET for short) molecule and its variants have played and, continue to play, a central role among molecular quantum materials. Besides superconductivity, many other interesting quantum phenomena occur in these salts, such as charge fluctuations, intermolecular charge-ordering, and ferroelectricity, spin liquids state and so forth [1–5]. Most salts have stoichiometry $(BEDT\text{-}TTF)_2^+X^-$ (X^- is a closed-shell anion), namely an electron every two BEDT-TTF, and the BEDT-TTF molecules are packed roughly upright, forming layers separated by sheets of anions or anion polymeric networks. The structure and physical properties are then quasi-two-dimensional (2D), and the interesting physics lie in the ET layers, with anion sheets just considered to serve as spacer and charge reservoir—although they may have a role in stabilizing the diverse electronic phases of the donor layer. The ET molecules can arrange in several different ways within the layers, even with the same counterions, yielding polymorphism associated with a variety of physical properties [6–8]; the different molecular packings being labeled by different Greek letters. The sharing of one electron between two molecular units favors the arrangement of ET in pairs, or dimers, within the layers. The degree of dimerization changes from almost nil in the case of the θ phase, to the chessboard arrangements of dimers of the κ phase.

ET salts are characterized by strongly correlated mobile electrons, and the interplay of competing but comparable interactions yield to several types of instabilities. Among the many different techniques used to probe the ET salts physical properties and investigate the resulting complex "phase diagram", a prominent role is played by vibrational spectroscopy, due to the strong coupling between electrons and phonons. In the case of ET, the most important phonons from this point of view are the three C=C stretchings, just because the HOMO orbital is mainly localized on the corresponding bonds (Fig. 1). Therefore, the removal of one electron weakens the bond, with large and practically linear downshift of the associated phonon frequency ($\gtrsim$100 cm^{-1}), yielding estimate of the average charge residing on the molecule [9,10]. Moreover, the two totally symmetric modes modulate the HOMO, and are then directly coupled to the electron (e-mv coupling), giving rise to very strong infrared (IR) bands. The comparison between Raman and infrared (IR) spectra thus yields an estimate of the e-mv coupling constants [11,12]. In addition, analysis of the band shape of the C=C stretching vibrations, notably the IR active b_{1u} ν_{27} (cf. Fig. 1), has yielded an estimate of the charge fluctuation velocity between ET molecules [13,14].

While both IR and Raman spectroscopy generally provide useful and complementary information, in case of ET salts, most attention, both theoretical and experimental, has been devoted to IR. There are several reasons for that, the main one being that measuring and calculating Raman intensities is complicated. There is also the problem of resonance or preresonance effects [15,16], with associated radiation absorption, fluorescence, etc. First-principles density functional (DFT)

*Contact author: girlando@momag.it

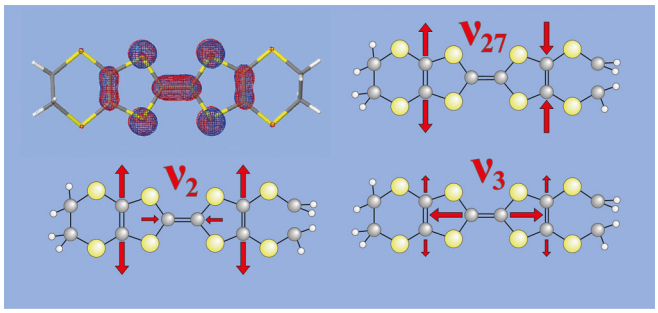

FIG. 1. BEDT-TTF HOMO orbital (upper left corner) and the three C=C stretching phonons, b_{1u} ν_{27}, a_g ν_2, and ν_3.

calculations were then limited to the IR intensities [10], and until recently just one paper tried to assign the Raman active C=C stretching of κ-phase ET salts through polarization measurements, isotopic substitution and the use of different excitation lines and temperatures [15]. Despite this outstanding effort, some interpretation remained uncertain (cf. Table III of the latter paper).

Recent high-quality polarized Raman spectra of κ-(BEDT-TTF)$_2$Hg(SCN)$_2$Cl (ET-HgCl for short) [17], a salt undergoing an intriguing reentrant charge order (CO) phase transition [17–19], have shown that the C=C stretching spectral region is more complex than generally thought. Considering the strong dimerization of κ-phase salts, and of this one in particular [20], I decided to perform DFT calculations of $(\text{BEDT-TTF})_2^+$ dimers along the lines sketched in Ref. [10], this time including calculation of the (nonresonant) Raman intensities of dimers keeping the same orientation as in the crystal, in order to reproduce the polarized measurement. Qualitative but quite satisfactory agreement with experiment, also considering the above sketched difficulties of assessing Raman intensities, prompts for a full reconsideration of the assignment of the Raman active C=C stretching phonons in κ-phase salts. Furthermore, the presence of a very broad band in the cross-polarized spectra is explained in terms of an effect of e-mv coupling involving interdimer interaction, allowing an evaluation of relevant Hubbard parameters. Finally, DFT calculation of a charge-ordered dimer gives important clues about the possible CO pattern in κ-(BEDT-TTF)$_2$Hg(SCN)$_2$Cl ferroelectric phase [20], and in others κ-phase salts displaying similarly originated phenomena [5].

II. METHODS

A. Spectral predictions

Table I reports the spectral predictions for the crystal phonons, using the correlation diagram that starts from the isolated molecule [21]. BEDT-TTF is not planar (D_2 symmetry [10]), but since here we are concerned with the three C=C stretchings, which constitute the planar part of the molecule, I shall follow the usual convention of classifying these phonons in terms of D_{2h} symmetry: For the isolated molecule, two stretching modes are Raman active (a_g ν_3 and ν_2), and one is IR active (b_{1u} ν_{27}). A cartoon of the three vibrations is reported in Fig. 1. In the crystal, the site symmetry of each ET is C_1, and in principle all the modes are both Raman and IR active. But the deviation from the isolated molecule symmetry is very small, so one expects that isolated molecule selection rule still apply. The two ET molecules in the dimer are connected by an inversion center, and each ET vibration is coupled in-phase and out-of-phase: For the C=C stretchings three IR active ($\mathcal{A}_u$) and three Raman active ($\mathcal{A}_g$) modes are expected. The three IR active modes have been identified: one is charge sensitive mode corresponding to the in-phase combination of the b_{1u} ν_{27}, and the other two are the e-mv coupled out-of-phase combination of a_g ν_2 and ν_3 [10]. On the other hand, in Raman the C=C stretching region is dominated by two strong bands, up to now identified as the in-phase

TABLE I. Correlation diagram for ET in-plane modes.

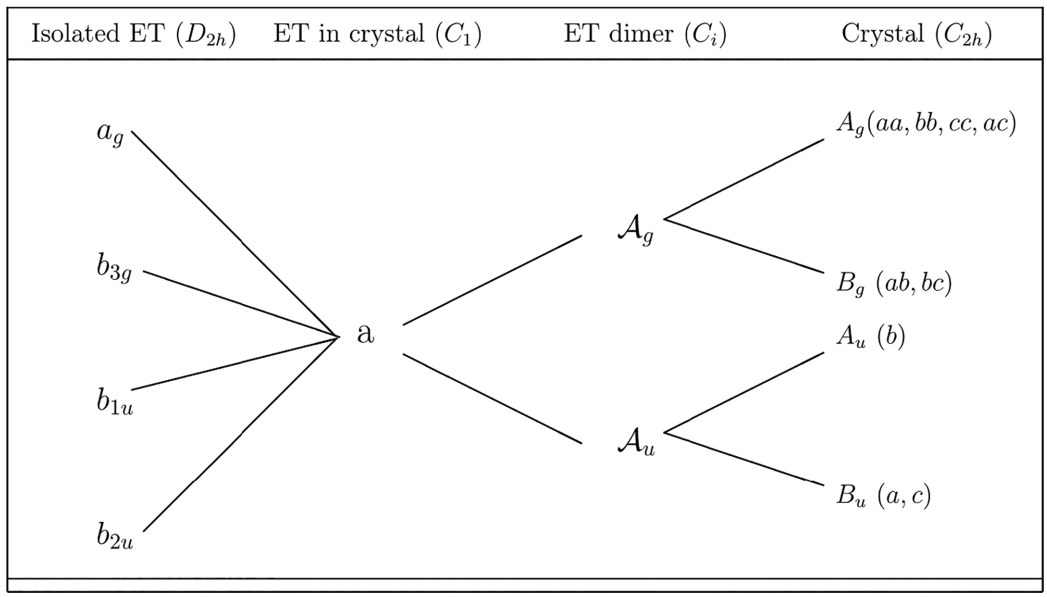

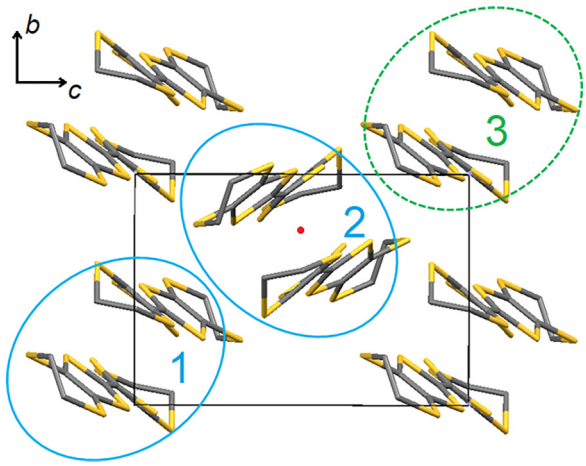

FIG. 2. Organic layer (*bc* plane) of ET-HgCl at 50 K. The continuous light-blue ellipses indicate the two dimers in the unit cell, the green-dashed line referring to the third dimer in the trimer cluster used for modeling the e-mv interaction. The red dot indicates the inversion center for both the dimer 2 and for the supermolecule trimer 123.

combination of the a_g ν_2 and ν_3, whereas the assignment of the b_{1u} ν_{27} remains uncertain [15].

The spectral prediction for the crystal phonons are obviously based on the crystal space group, or to be precise, on the corresponding factor group [21]. Of course, different κ-ET salts may crystallize in different space group, so for instance ET-HgCl crystal is monoclinic $C2/c$ (C_{2h}^5) [18], with four $(ET)_2^+$ dimers in the unit cell (i.e., two dimers in the primitive cell), whereas κ-$(ET)_2Cu[N(CN)_2]Br$ is orthorhombic, *Pnma* (D_{2h}^{16}) with four dimers in the unit cell [15]. Therefore, in ET-HgCl each dimer band splits into two, and in κ-$(ET)_2Cu[N(CN)_2]Br$ it splits into four. However, since the four dimers are arranged into two pairs located in different layers separated by the counterions, their interaction is expected to be negligibly small, and the four bands to be degenerate two by two [15]. Here, I adopt the view that what it is important for the spectral predictions is the structure of the 2D organic *layer* rather than the whole crystal, the arrangement of ET molecules within the layer being the motif common to all κ salts. Figure 2 show the typical chessboard packing of ET dimers within the layer, whose 2D symmetry would be *Pgg*, to which the C_{2h} factor group is associated. Thus, as shown from the right side of Table I, each dimer phonon is coupled in-phase and out-of-phase, giving rise to Raman active A_g and B_g Davydov components, and the corresponding IR active A_u and B_u components.

B. Quantum chemical calculations

Quantum chemical calculations have been performed with the GAMESS package [22] version 2022 R2, using DFT-B3LYP, and the 6-31G(d) basis set, following the previously adopted protocol [10]. The initial dimer geometry was taken from the 10 K structure of ET-HgCl [18], imposing the D_2 geometry for ET, and the inversion symmetry to $(ET)_2^+$ dimer, so the charge is equally shared among the two molecules. In order to simulate the Raman polarization measurements, I had to postprocess the GAMESS output to extract the component of the Raman polarizability tensor along the *xyz* coordinates of the dimer. The oriented gas model [21] is then used to predict the A_g and B_g Raman polarization intensities (cf. Table I). In oriented gas model the two dimers are assumed to be completely noninteracting: The bands occur at the same frequency, but the intensities are proportional to the square of the relevant polarizability component along the crystal axes,

$$\boldsymbol{\alpha}_{A_g} = \mathbf{T}\boldsymbol{\alpha}_{d1}\mathbf{T}^{\mathrm{t}} + \mathbf{T}\boldsymbol{\alpha}_{d2}\mathbf{T}^{\mathrm{t}}, \tag{1}$$

$$\boldsymbol{\alpha}_{B_g} = \mathbf{T}\boldsymbol{\alpha}_{d1}\mathbf{T}^{\mathrm{t}} - \mathbf{T}\boldsymbol{\alpha}_{d2}\mathbf{T}^{\mathrm{t}}, \tag{2}$$

where $\boldsymbol{\alpha}_{d1}$, $\boldsymbol{\alpha}_{d2}$ are the polarizability tensors of dimer 1 and 2 (Fig. 2), expressed in the dimer *xyz* coordinates, and $\mathbf{T}$ ($\mathbf{T}^t$) are the transformation matrix (its transpose) between the dimers' *xyz* coordinates and the crystal *abc* coordinates (assumed orthogonal, since in ET-HgCl the β angle is very close to 90° [18]). All intensities are *relative* intensities, as in the experiments. Finally, in order to simulate the spectra of ET-HgCl in the CO state [17,18], the constrain of the dimer inversion center has been removed, and an electric field of 0.001 a.u. directed along the two molecular barycenters has been applied, in such a way to induce the required charge separation.

C. Trimer model for interdimer e-mv interaction

As stated above, the oriented gas model used to simulate the crystal Raman spectra considers interdimer interactions as negligible, yielding at most a few wavenumber splitting. This assumption is in general satisfied in molecular crystals, but in the present case I have realized that e-mv interaction *between dimers*, rather than inside the dimer, originates quite sizable splitting clearly observable in Raman spectra. The effect has been recognized in κ-$(BEDT\text{-}TTF)_2Cu_2(CN)_3$ [23], but not analyzed. To account for it I developed a suitable model along the lines proposed many years ago [11,12,24,25] for e-mv interaction in CT crystals. The detailed development of the model is reported in the Appendix A, here the basic outline is presented.

At the core of traditional e-mv models there is the modulation of frontier molecular orbital by the totally symmetric (a_g) molecular phonons. If the dimer is considered as a supermolecule, disregarding the internal degrees of freedom, it is easy to realize that the in-phase coupled a_g modes ($\mathcal{A}_g$, cf. Table I) modulate the supermolecule frontier orbital, and give rise to interdimer e-mv effects. In order to properly simulate the Raman e-mv effects, a cluster made up of three dimers is used, in such a way to preserve the inversion center between the dimers, as sketched in Fig. 2. The relevant cluster trimeric Hubbard Hamiltonian therefore is ($\hbar = 1$, $i = 1 - 3$)

$$H_e = \sum_i \varepsilon_0 n_i + \frac{U}{2}\sum_{i,\sigma} n_{i,\sigma}n_{i,-\sigma} + t\sum_{\sigma}(c^+_{1,\sigma}c_{2,\sigma} + c^+_{2,\sigma}c_{1,\sigma} + c^+_{2,\sigma}c_{3,\sigma} + c^+_{3,\sigma}c_{2,\sigma}), \tag{3}$$

where $c^+_{i,\sigma}$ and $c_{i,\sigma}$ denote site i creation and destruction operators for electron with spin σ, $n_{i,\sigma} = c^+_{i,\sigma}c_{i,\sigma}$, $n_i = \sum_\sigma n_{i,\sigma}$ is the corresponding occupation number operator. ε_0 is the energy of the supermolecule frontier orbital, U is the effective

repulsion energy between two paired electrons on the same orbital, and t is the interdimer hopping integral $t = t_{12} = t_{23}$.

The above is the purely electronic Hamiltonian. The vibrational Hamiltonian is

$$H_v = \sum_{i,m} \frac{1}{4}\left(\dot{Q}^2_{i,m} + Q^2_{i,m}\right)\omega_m \tag{4}$$

with m counts the supermolecule $\mathcal{A}_g$ dimensionless normal coordinates Q_m. Finally, the e-mv Hamiltonian is written as

$$H_{e-mv} = \sum_{m,i} g_m n_i Q_{i,m} \tag{5}$$

where g_m is the e-mv coupling constant, i.e., the derivative of the supermolecule frontier orbital with respect to the relevant $\mathcal{A}_g$ normal coordinate.

The center of inversion symmetry is exploited by introducing the following number operators:

$$N_{\mathrm{TOT}} = n_1 + n_2 + n_3 \quad = 3, \tag{6}$$

$$\mathcal{N}_s = 2n_2 - (n_1 + n_3), \tag{7}$$

$$\mathcal{N}_a = n_1 - n_3, \tag{8}$$

and symmetry adapted normal coordinates

$$S_m = Q_{1,m} + Q_{2,m} + Q_{3,m}, \tag{9}$$

$$s_m = 2Q_{2,m} - (Q_{1,m} + Q_{3,m}), \tag{10}$$

$$q_m = Q_{1,m} - Q_{3,m}. \tag{11}$$

N_{TOT} is the total number of electrons distributed over the trimer cluster and is a constant of motion. The corresponding coordinate S_m is decoupled from the electronic system. $\mathcal{N}_a$ and q_m account for the effects of interdimer e-mv perturbation in IR, and will not be discussed in the present paper, whereas $\mathcal{N}_s$ and s_m account for the e-mv effect in Raman. The zero-frequency Raman susceptibility $\chi_R(0)$ is given by

$$\chi_R(0) = \sum_{\mu} \frac{2\langle\mu|\mathcal{N}_s|0\rangle^2}{\omega_{\mu 0}}. \tag{12}$$

where $\omega_{\mu 0} = E_\mu - E_0$ and $|\mu\rangle$ and E_μ are the eigenstates and eigenvalues of the electronic Hamiltonian (3), $\mu = 0$ labeling the ground state. Finally, in the isolated band approximation [26], the frequency shift due to e-mv perturbation is

$$\omega_m^2 - \Omega_m^2 = g_m^2 \omega_m \chi_R(0), \tag{13}$$

where ω_m and Ω_m are the unperturbed and perturbed frequency of the supermolecule mth $\mathcal{A}_g$ phonon.

III. RESULTS

A. ET-HgCl metallic state

Figure 3 shows the calculated total IR and Raman intensities of $(ET)_2^+$ C=C stretching vibrations for a pair of noninteracting dimers arranged in the chessboard pattern typical of κ-phase ET salt.

The chosen bandshape is a Lorentzian, with 1 cm^{-1} bandwidth in order to have clearly separated peaks. Other modes, like the CH bendings, are included in the simulation, but the

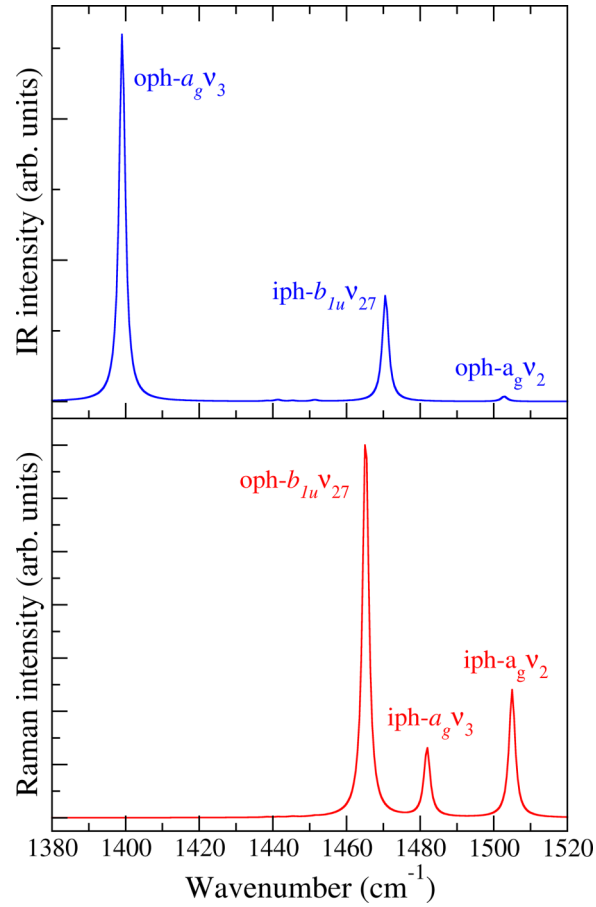

FIG. 3. Simulated IR and Raman spectra of ET-HgCl powders in the C=C stretching region. The C=C bands assignment refers to the conventional labeling relevant of a single ET molecule, the preceding oph and iph standing for out-of-phase and in-phase coupling of the molecular vibration in the ET dimer.

spectra are dominated by six bands, three in IR and three in Raman, corresponding to the in-phase (iph) and out-of-phase (oph) coupling of the three vibrations depicted in Fig. 1.

The simulated IR spectra of $(ET)_2^+$ have been already reported in Ref. [10]; here only a brief comment is in order. The iph-b_{1u} ν_{27} is the charge sensitive mode often used to determine the ET charge [10,18], whereas the two oph modes are the e-mv induced vibrations, displaying frequency lowering with respect to the corresponding iph modes, and intensity borrowing from the nearby CT electronic transition [11]. It is known that DFT-B3LYP calculations do not model very well intermolecular and CT interactions. In particular, the effects of intradimer e-mv interaction are only partially captured, as the calculated shifts and intensity borrowing are highly underestimated [10]. In the present case, the experimental frequency of e-mv induced oph-a_g ν_3 is located around 1200 cm^{-1} in ET-HgCl [18], whereas the calculation places it around 1400 cm^{-1}. Also notice that according to calculations the intensity and frequency lowering of the oph-a_g ν_2 are much lower than those of the a_g ν_3. This is due to the fact that the two modes are strongly mixed through the coupling to CT transition, and their behavior can be easily understood in terms of ordinary perturbation theory [12]. To simplify the

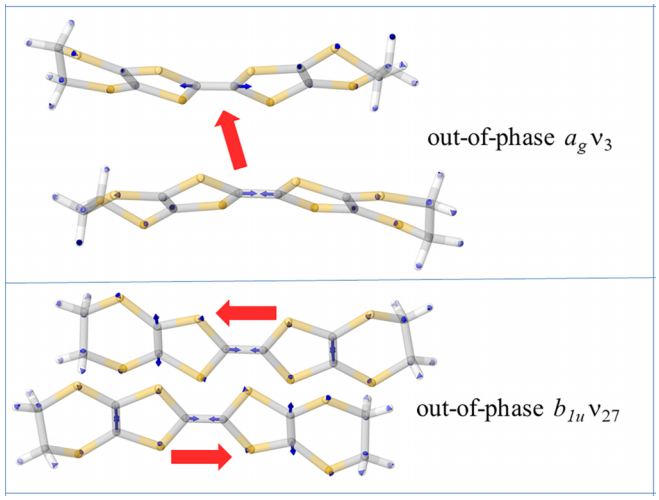

FIG. 4. (Top) Eigenvectors of the IR active, out-of-phase coupled $a_g\ \nu_3$. (Bottom) Eigenvectors of the Raman active, out-of-phase $b_{1u}\ \nu_{27}$. The arrows indicate the direction of the oscillating dipole moments.

following discussion, we shall focus attention mainly on the oph-$a_g\ \nu_3$, whose eigenvectors are sketched in upper panel of Fig. 4. The red arrow indicates the direction of the (strong) intermolecular oscillating dipole moment, corresponding to back and forth charge flux [11].

Now we analyze the simulated Raman spectra reported in the lower panel of Fig. 3, where an unforeseen result is evidenced. In fact, three bands are present, the most intense being associated to the out-of-phase coupling of the $b_{1u}\ \nu_{27}$. Of course, selection rules predict that this *ungerade* molecular vibration becomes Raman active in the dimer, but its high intensity was not expected. And since the Raman spectra of κ-ET salts were dominated by two bands, these were associated to the two ip-a_g vibrations [15], since totally symmetric modes generally are the most intense in the spectra. On the other hand, *a posteriori* reasoning well accounts for the results of calculations: The $b_{1u}\ \nu_{27}$ has strong IR intensity, only surpassed by some e-mv induced modes, which means strong oscillating dipole moment along the long ET molecular axis. And the antiphase oscillation of two parallel dipole moments, as depicted in the bottom panel of Fig. 4, means strong polarizability modulation, i.e., strong Raman intensity.

The assignment of the C=C Raman bands in ET κ phase has to be reconsidered in light of the above result. In Fig. 5 we compare the experimental polarized Raman spectra of ET-HgCl on the (*bc*) plane in the metallic phase [17] with the calculated one, where $4\,\mathrm{cm}^{-1}$ bandwidth for the Lorentzians has been applied. We first underline that the simulation reproduces properly the difference in intensity between the spectra recorded with parallel (*cc*) and crossed (*bc*) polarization, the latter being approximately four to five times less intense than the former. The relative intensity within one polarization does not agree very well with experiment, but precise agreement is not to be expected. On one hand, calculations are of course approximate, and do not consider the effects of resonance on the Raman intensities, which is certainly present with the employed 514-nm exciting line (cf. Ref. [15] for the effects

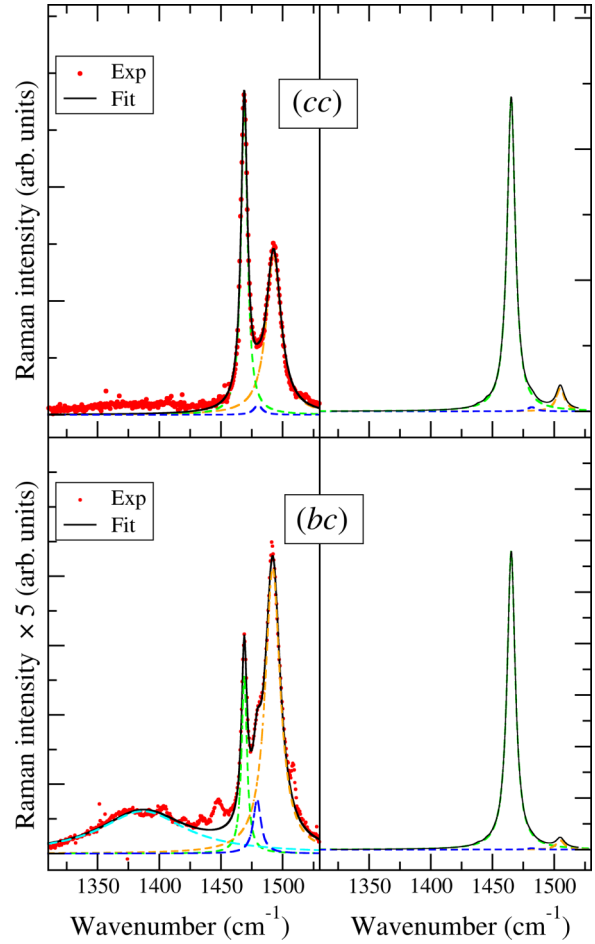

FIG. 5. (Left panels) ET-HgCl experimental polarized Raman spectra at 50 K (from Ref. [17]; exciting line: 514 nm). (Right panels) Calculated spectra. The Raman intensities are in arbitrary units, but the scale of the both the (*bc*) spectra is multiplied by a factor of $\approx$ 5. The dashed orange, blue, green, and cyan lines represent the band deconvolution assuming Lorentzian band shape.

of different exciting lines on the Raman spectra of ET salts). Moreover, the experimental Raman intensity measurements are delicate, with difficult to control effects related not only to resonance, but also crystal imperfections, etc. In any case, the simulated spectra give an important information, namely that the ip-$a_g\ \nu_3$ intensity is greatly reduced in the generally used collection geometry (backscattering observation on the most developed crystal plane, corresponding to the ET layers). Therefore, the ip-$a_g\ \nu_3$ is almost completely masked by the nearby oph-$b_{1u}\ \nu_{27}$, especially in the parallel or unpolarized spectra, so that only two Raman bands are generally observed in this spectral region. The robustness of this results has been checked by changing DFT functional and basis set.

The precise interpretation of the crossed polarization (*bc*) spectra of ET-HgCl is more complicate, as several bands are clustered in the $1450 - 1520\,\mathrm{cm}^{-1}$ spectral region. In addition, there is a fourth band, centered around $1387\,\mathrm{cm}^{-1}$, very broad, but with a total intensity comparable to that of the other bands. This peculiar Raman band is found in other κ-phase salts, like for instance κ-(BEDT-TTF)$_2$Cu(NCS)$_2$ [27] or κ-(BEDT-TTF)$_2$Cu[N(CN)$_2$]Br [15], albeit at frequencies

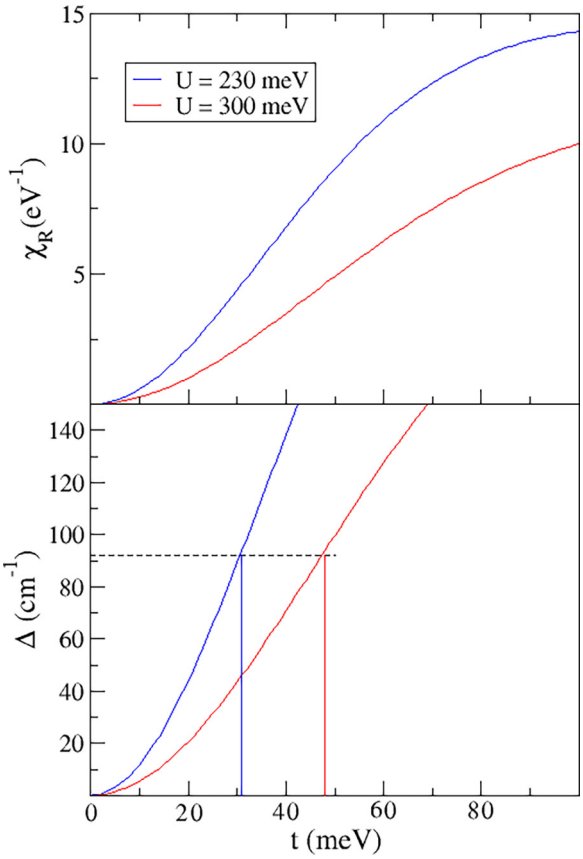

FIG. 6. Results of the trimer model. (Top) $\chi_R(t)$ for two different values of U. (Bottom) t dependence of $\Delta = \omega_{\nu 3} - \Omega_{\nu 3}$. The dashed-horizontal line marks the position of the experimental $\Delta = 92$ cm^{-1} for ET-HgCl at 50 K (from left-bottom panel of Fig. 5).

different in different salts. Isotopic substitution of the central C=C carbon atoms [15] shows that this band is associated to the crystalline B_g component corresponding to the $a_g\,\nu_3$ molecular mode (Table I). The question now is: Why this component displays such an unusually large splitting with respect to A_g component, that from the above analysis is located at 1479 cm^{-1}?

The answer is that the large splitting is a manifestation *inter*dimer e-mv coupling, as proposed in the case of κ-(BEDT-TTF)$_2$Cu$_2$(CN)$_3$ [23]. Of course, the splitting cannot be reproduced by the above DFT calculations, relevant to noninteracting dimers, and likely not even by very heavy calculations for the vibrations of the unit cell molecule.

As already explained in Sec. II C and depicted in Fig. 2, in order to deal specifically with interdimer e-mv interaction I have developed a trimer model, the trimer being made up by $(ET)_2^+$ dimers. Appendix A reports the solution of the model: The electronic Hamiltonian of Eq. (3) is solved numerically for different values of the U/t ratio, and so is the Raman susceptibility, whose t dependence for two different values of U is reported in the top panel of Fig. 6. We then use Eq. (13) with $g_{\nu 3} = 71$ meV [10] to calculate $\Delta = \omega_{\nu 3} - \Omega_{\nu 3}$, as reported in the bottom panel of Fig. 6. By taking the experimental $\Delta = 92$ cm^{-1} we get $t = 31$ meV for $U = 230$ meV or $t = 48$ meV for $U = 300$ meV, values compatible (considering all the made approximations) with those calculated in the framework of the effective dimer model [20].

The effective dimer model [28–30] is often used to analyze the phase diagram of κ-phase ET salts. Indeed, the two parameters of the model Hamiltonian (3) correspond to two of the four parameters of the effective dimer model (see Appendix A). The study here, making reference to just one experimental datum, can only give the ratio between the two parameters, and here we shall not go beyond the demonstration of the e-mv origin of the 1387 cm^{-1} Raman band. But the discovery of the effect opens the way to the possible experimental estimate of all the κ-phase effective dimer model parameters *via* optical spectroscopy.

B. ET-HgCl charge ordered state

Among κ-phase salts, ET-HgCl is unique in displaying a CO phase transition around 30 K, as detected by both IR [18] and Raman [17] spectroscopy. With the aim of shedding light into the transition mechanism and physical consequences, I decided to simulate the vibrational spectra of ET-HgCl in the CO state, following the generally accepted idea that the CO or disproportionation occurs inside the dimer. Therefore I removed the constraint of the inversion center in the dimer, that assured equally distributed charge between the two ET moieties, at the same applying an electric field along the molecular barycenters to induce the experimentally observed $0.2e$ charge difference (cf. Sec. II B). Spectral predictions say that by removing the inversion center all the modes becomes both IR and Raman active, so, disregarding the Davydov splitting, we expect six C=C bands occurring at the same frequency in IR and Raman. Of course, this is precisely what we obtain in the simulation, but with the advantage of information about the intensity distribution, as shown in Fig. 7, where the simulated spectra of the powders are reported for both the symmetric and CO dimer.

The band labeling of Fig. 7 is the the same as Fig. 3, with omission of the "oph" and "iph" prefixes to avoid label crowding. In the CO phase (red line), the "+" and "−" superscripts refer to charge rich and charge poor molecule within the dimer. We first examine the IR spectra in the top panel of the figure. Here we see that the calculated 35 cm^{-1} splitting of the charge sensitive ν_{27} is in line with the experimental one (29 cm^{-1} [18]), indicating that the simulation correctly reproduces the actual charge separation. The ν_{27} splitting is observed in the polarization perpendicular to the ET layer, i.e., the *bc* plane. On the other hand, the experimental spectra along *b* and *c* are dominated by the e-mv coupled mode ν_3 and the nearby CT electronic transition, and become very complicated below the phase transition [18]. The calculation indicates that ν_3^- is downshifted only by a few wavenumbers with respect to the ν_3 of the metallic phase (dashed-blue line in the figure), while the ν_3^+, whose intensity is predicted to be much lower, is close to the almost undetectable $\nu_2^\pm$. We have already remarked in Sec. III A that the calculated frequency of the ν_3 ($\sim$1400 cm^{-1}) is much higher than the observed one (1200 cm^{-1}) [18].

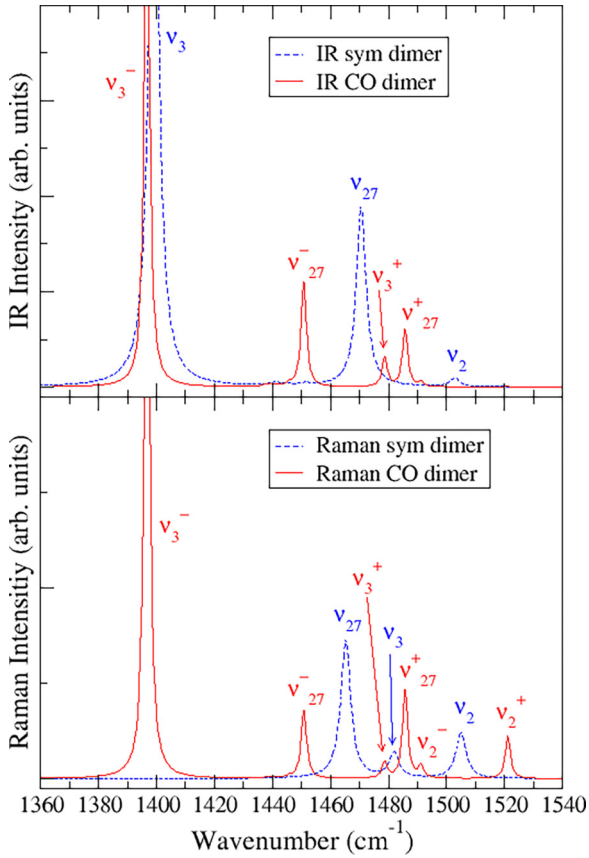

FIG. 7. Calculated IR and Raman spectra of ET-HgCl powders in the C=C stretching region above and below a hypothetical CO phase transition, i.e., a symmetric dimer (dashed-blue line) and a CO dimer (red line). The mode labeling is the same as in Fig. 3, and in the CO phase the plus and minus refer to charge rich and charge poor molecule.

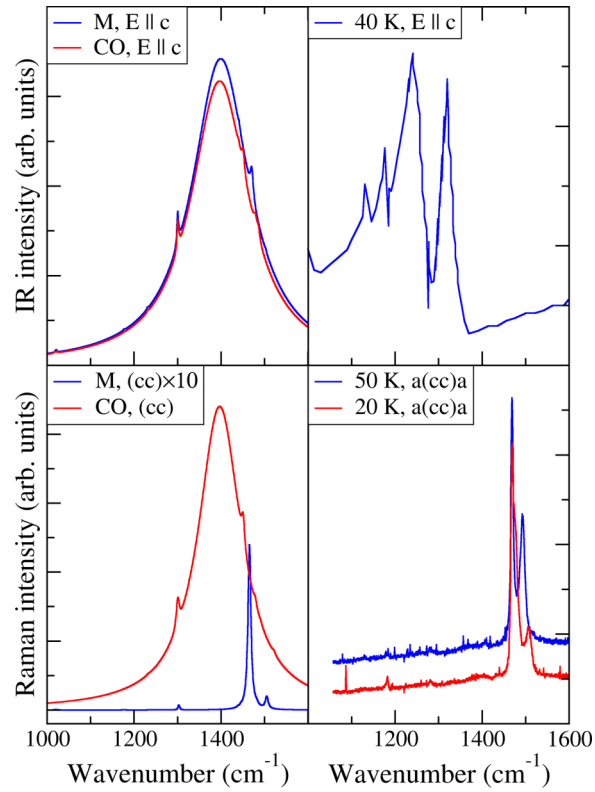

FIG. 8. (Left panels) Simulated polarized Raman and IR spectra of ET-HgCl in the metallic (M) and CO phases (blue and red lines, respectively). The simulated spectra assume charge ordered, non symmetric dimers. (Right panels) Experimental IR and Raman spectra above and below the CO transition (blue and red lines, respectively). The experimental spectra are from Refs. [18] and [17]. Raman exciting line: 514 nm.

In the simulated Raman spectra (bottom panel of Fig. 7) we again notice that the splitting of the charge sensitive ν_2 mode, 30 cm^{-1}, is in line with the experiment (32 cm^{-1} [17]), whereas the remaining $1440 - 1500\,cm^{-1}$ spectra region is very crowded. Before embarking in the comparison with the corresponding experimental spectra, it is useful to focus on a very important and unambiguous information provided by the simulation, namely, the appearance with huge intensity the e-mv coupled, out-of-phase $a_g\nu_3^-$ (top panel of Fig. 4). Elementary group theory just predicts that all the IR active modes, forbidden in the symmetric dimer (metallic phase) become also Raman active if the dimer inversion center is lost. Perhaps the huge Raman intensity is overestimated in a calculation made in the presence of an external electric field, but after all this finding parallels the high intensity of the out-of-phase $b_{1u}\,\nu_{27}$: In both cases we have strong charge oscillation with corresponding oscillating dipole moment, reflecting in equally strong oscillating polarizability.

Therefore, according to the simulation, if ET-HgCl CO transition involves differently charged molecules *within* the dimer, we should observe the insurgence of a strong Raman band in correspondence with the IR e-mv induced $a_g\,\nu_3$. In order to verify the above, in Fig. 8 we compare the simulated crystal Raman spectra of symmetric and CO dimers with the experimental ones above and below the phase transition. We have chosen the (*cc*) polarization, where the out-of-phase $a_g\nu_3$ should appears with the highest intensity. In the simulated spectra (left side of Fig. 8) we have used Lorentzian bandshape with bandwidth adjusted to simulate the experiment.

The upper-right panel of Fig. 8 reports the experimental conductivity spectrum in the metallic phase (digitized from Ref. [18]). The one in the CO state is not reported since at the phase transition the reflectivity goes down drastically and the optical conductivity spectral weight shifts from the zero-frequency peak to a new maximum at about 700 cm^{-1} [18], overlapping the $a_g\nu_3$. But its position is substantially unaltered, as confirmed by the simulated spectra. Finally, we recall that the experimental IR bandshape of the $a_g\nu_3$ is not a Lorentzian, but it has rather a Fano-like aspect, with Fano indentations in correspondence with the underlying CH bending modes [31].

The right-bottom panel of Fig. 8 shows that the experimental Raman spectra in the frequency region of the out-of phase $a_g\nu_3$ are completely flat above the phase transition, at it should be, but remain precisely the same below. We are then led to the conclusion that the intradimer inversion center is retained in the CO phase. In other words, and contrary to the assumption at the basis of the present DFT simulation, the charge separation is *not* between the two moieties of the

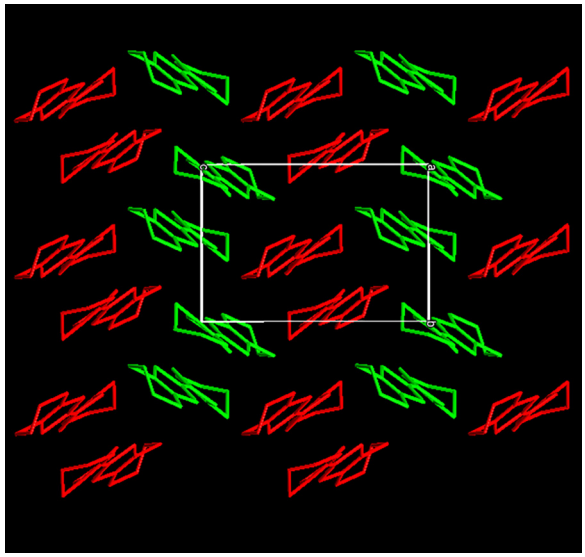

FIG. 9. Suggested crystal structure of ET-HgCl in the CO phase. Symmetry (inversion center) related dimers are drawn in the same color, red, or green. The red and green colors correspond to differently charged dimers. Hydrogens are not shown.

dimer, but between the dimers. In this case, the symmetry descent from the $C2/c$ crystal structure [18] necessarily yields to the $P\bar{1}$ structure, with two nonequivalent dimers per unit cell (Fig. 9).

The above indication contrasts with the intradimer disproportionation proposed early on the basis of electronic and magnetic data [17,18,20]. Of course, if a band goes undetected for some reason (e.g., resonance Raman effects, screening by the electronic response, etc.), it does not mean the band is not present, also because this spectral region has not be considered informative so far, and has not been deeply investigated. On the other hand, evidences in favor of the intradimer CO depend on interpretation of electronic and magnetic data, whereas the presence/absence of the $a_g\nu_3^-$ in Raman is bound to a strict, symmetry based selection rule (the well known "rule of mutual exclusion" of vibrational spectroscopy). Another indication in favor of the present finding comes from what has been found on another κ-phase salt, the widely studied spin-liquid candidate κ-(BEDT-TTF)$_2$Cu$_2$(CN)$_3$ [32]. A very accurate crystal structure determination [33] has shown a small *inter*dimer average charge difference, 0.06 ± 0.05, and according to a recent paper [34] no strong Raman band seems to be present around $1200\,\mathrm{cm}^{-1}$, in correspondence with the IR e-mv induced $a_g\nu_3$. Another intuitive argument in favor of the interdimer CO is that the itinerant electrons jump more easily and quickly between more strongly interacting molecules, and in the present case the intradimer hopping integral is about twice the interdimer one [20].

Of course it is impossible to make a computational simulation of the Raman spectra of a interdimer charge-ordered κ phase to compare with the experiment. A tentative, but successful interpretation of whole C=C stretching region of ET-HgCl Raman spectra in CO state based on the assumption that the spectra are a superposition of (BEDT-TTF)$_2^{+0.6}$ and (BEDT-TTF)$_2^{+0.4}$ symmetric dimers is reported in Appendix B.

IV. CONCLUSIONS

First-principles calculations of the Raman intensities of (BEDT-TTF)$_2^+$ dimers oriented as in ET-HgCl crystal lead to reconsider the assignment of the corresponding Raman spectra in the critical region of BEDT-TTF C=C stretching. Although group theory predicts that in a dimer the out-of-phase coupling of the IR active b_{1u} ν_{27} becomes Raman active, no one expected that the corresponding band should have such a strong Raman intensity, likely obscuring the in-phase coupling of the a_g ν_3 (cf. Figs. 3 and 5). An intuitive justification of this finding is based on the fact that the b_{1u} ν_{27} implies large charge oscillation in the direction of the BEDT-TTF long molecular axis [10], leading to strong Raman intensity for the corresponding antiphase charge oscillation (bottom panel of Fig. 4).

In the reanalysis of the C=C stretching Raman spectra, I have also been able to identify the origin of a broad band appearing in the cross polarized spectra about $90\,\mathrm{cm}^{-1}$ lower than the a_g ν_3. This band is typical of the κ-phase salts, and it has been already assigned to the B_g component of A_g phonon associated to a_g ν_3 stretching [15]. We explain the unusually large Davydov splitting as a manifestation of interdimer e-mv coupling. By adapting the Rice's model of e-mv coupling [11] to the present case, I show how optical data can be used to extract relevant parameters of the effective dimer model [28–30] often adopted to explain the physical properties of κ-phase ET salts.

Finally, this paper reports the simulated Raman spectra of the CO ferroelectric phase of ET-HgCl [17,18] following the generally accepted idea that the CO implies the breaking of the intradimer inversion center symmetry. In such a case it is obvious that the IR active phonons become also Raman active and vice versa, as observed in another quite different ET salt, θ-(BEDT-TTF)$_2$TlZn(SCN)$_4$ [35]. What the calculations do again tell us, however, is the huge Raman intensity acquired by the out-of-phase coupling of the a_g ν_3. This phonon has huge IR intensity due to the intermolecular charge oscillation induced by the e-mv coupling [11] (cf. the top panel of Fig. 4), and as in the case of b_{1u} ν_{27}, should give rise to equally large Raman intensity. The lack of the appearance of such a band in correspondence with ET-HgCl CO phase transition (cf. Fig. 8) implies that the intradimer inversion center symmetry is not broken, strongly suggesting that the CO pattern (Fig. 9) is different from the one hypothesized so far [18]. The above finding is likely the most important obtained here, and I believe it will stimulate the Raman collection and reanalysis of other κ-BEDT-TTF and BETS salts (BETS is bis-ethylenedithio-tetraselenafulvalene), that constitute a widely investigated family of frustrated Mott systems [5].

ACKNOWLEDGMENTS

I gratefully thank Prof. N. Drichko (John Hopkins Baltimore), Prof. M. Dressel (Stuttgart University), and Prof. M. Masino and A. Painelli (Parma University) for the many

useful discussions and critical reading of the manuscript. I also thank N. Drichko for calling my attention to the problem and providing the original and in part unpublished spectra of ET-HgCl .

APPENDIX A: TRIMER MODEL FOR INTERDIMER E-MV COUPLING

The first step is to solve the electronic Hamiltonian (3). The basis set is constructed by distributing three spins on the three dimer sites. There are 20 ways of distributing the spins, four constitute a quartet ($S = 3/2$) and 16 are doublets ($S = 1/2$), eight states correspond to different spin arrangements with one electron per site, as summarized in Table II.

Since we are not concerned with the spin, but only with the distribution of the three charges following the Pauli exclusion principle, we can take as basis functions just the ones with the same $S_z = 1/2$ (marked in bold in the table). In this way the basis function set is reduced to seven, ϕ_1 to ϕ_7. Identical result can be obtained in simpler way by using a spinless fermion approach. Adopting the symbols ○, ⊛, and ● for empty site, single, and double occupancy, respectively, the resulting seven basis wave functions can be written as $\phi_1 = |\circledast\circledast\circledast\rangle$, $\phi_2 = |\bullet\circ\circledast\rangle$, $\phi_3 = |\bullet\circledast\circ\rangle$, $\phi_4 = |\circledast\bullet\circ\rangle$, $\phi_5 = |\circ\bullet\circledast\rangle$, $\phi_6 = |\circ\circledast\bullet\rangle$, and $\phi_7 = |\circledast\circ\bullet\rangle$.

We can exploit the center of inversion to construct symmetry adapted wavefunctions,

$$\psi_1^{(+)} \equiv \phi_1.$$
$$\psi_2^{(+)} = (1/\sqrt{2})\{\phi_3 + \phi_6\}.$$
$$\psi_3^{(+)} = (1/2)\{[\phi_5 + \phi_4] + [\phi_2 + \phi_7]\}.$$
$$\psi_4^{(\mp)} = (1/2)\{[\phi_5 + \phi_4] - [\phi_2 + \phi_7]\}.$$

TABLE II. Possible distribution of three electrons on three sites.

n	Site 1	Site 2	Site 3	S_z	Wavefunction
1	↑	↑	↑	3/2	
2	↓	↓	↓	–3/2	
3	↑	↑	↓	1/2	
4	↓	↓	↑	–1/2	
5	↑	↓	↑	1/2	ϕ_1
6	↓	↑	↓	–1/2	
7	↓	↑	↑	1/2	
8	↑	↓	↓	–1/2	
9	↑↓	0	↑	1/2	ϕ_2
10	↑↓	0	↓	–1/2	
11	↑↓	↑	0	1/2	ϕ_3
12	↑↓	↓	0	–1/2	
13	↑	↑↓	0	1/2	ϕ_4
14	↓	↑↓	0	–1/2	
15	0	↑↓	↑	1/2	ϕ_5
16	0	↑↓	↓	–1/2	
17	0	↑	↑↓	1/2	ϕ_6
18	0	↓	↑↓	–1/2	
19	↑	0	↑↓	1/2	ϕ_7
20	↓	0	↑↓	–1/2	

$$\psi_5^{(\pm)} = (1/2)\{[\phi_5 - \phi_4] + [\phi_2 - \phi_7]\}.$$
$$\psi_6^{(-)} = (1/\sqrt{2})\{\phi_3 - \phi_6\}.$$
$$\psi_7^{(-)} = (1/2)\{[\phi_5 - \phi_4] - [\phi_2 - \phi_7]\}. \quad \text{(A1)}$$

On this basis the electronic Hamiltonian (3) is block diagonal ($\varepsilon_0 = 0$),

$$\begin{bmatrix} 0 & 0 & 2t & 0 & 0 & 0 & 0 \\ 0 & U & \sqrt{2}t & 0 & 0 & 0 & 0 \\ 2t & \sqrt{2}t & U & 0 & 0 & 0 & 0 \\ 0 & 0 & 0 & U & 0 & 0 & 0 \\ 0 & 0 & 0 & 0 & U & 0 & 0 \\ 0 & 0 & 0 & 0 & 0 & U & -\sqrt{2}t \\ 0 & 0 & 0 & 0 & 0 & -\sqrt{2}t & U \end{bmatrix}. \quad \text{(A2)}$$

The 3×3 block can be easily diagonalized symbolically only for $U = 0$, with roots $E_1 \equiv E_{GS} = -\sqrt{6}t$, $E_3 = 0$ and $E_7 = \sqrt{6}t$. The 2×2 block gives $E_2 = U - \sqrt{2}t$ and $E_6 = U + \sqrt{2}t$, while the $E_4 = E_5 = U$. The numerical solution for the energies as a function of U for $t = 1$ are reported in Fig. 10.

The ground-state wavefunction is

$$\Psi_{GS} \equiv \Psi_1 = c_1\psi_1^{(+)} + c_2\psi_2^{(+)} + c_3\psi_3^{(+)}, \quad \text{(A3)}$$

and the operator (7) connects the ground state with $\Psi_4 \equiv \psi_4^{(\mp)}$ only, so that the Raman susceptibility (12) is given by

$$\chi_R = \frac{2\langle\Psi_4|\mathcal{N}_s|\Psi_{GS}\rangle^2}{U - E_{GS}} = \frac{18c_3^2}{U - E_{GS}}. \quad \text{(A4)}$$

The top panel of Fig. 6 reports $\chi_R(t)$ for two different values of U.

In Fig. 11 we show a cartoon with an intuitive picture of the interdimer e-mv mechanism. Q_1, Q_2, and Q_3 are the normal coordinates (relative to iph-a_g ν_3) that combined in antiphase (B_g, Table I) yield the s_m coordinate [Eq. (10)]. This coordinate, modulating the dimers frontier orbitals in antiphase, is coupled to the symmetric interdimer CT, as sketched by the greenish arrows, thus lowering the corresponding vibrational frequency.

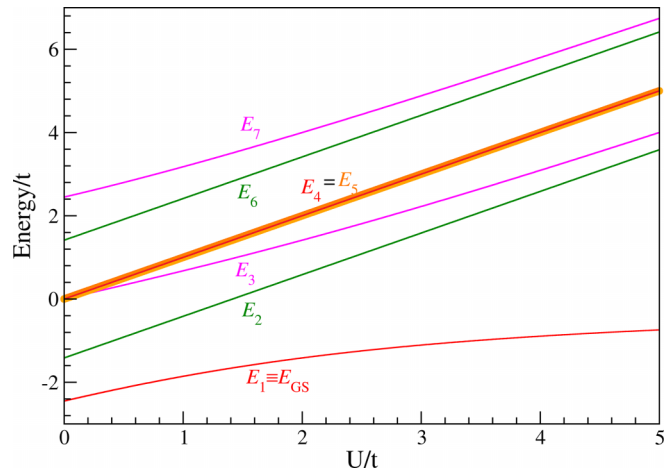

FIG. 10. Trimer energy levels as a function of U, in t units ($\varepsilon_0 = 0$).

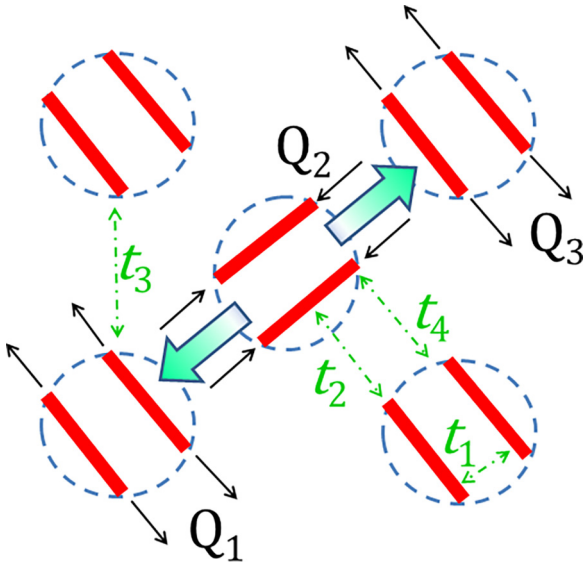

FIG. 11. Cartoon of the e-mv mechanism yielding to the observed Raman effect. The definition of the four intermolecular hopping integrals $t_1 - t_4$ is also shown. Within the effective dimer model $U_{\rm eff} = 2t_1, t = (t_2 + t_4)/2, t' = t_3/2$.

In the same figure we report the definition of the intermolecular hopping integrals t_1 (between the two molecules in the dimer), t_2, t_3, and t_4. In the framework of the effective dimer model [28–30] we have $U_{\rm eff} = 2t_1, t = (t_2 + t_4)/2$, $t' = t_3/2$. Obviously, $U_{\rm eff}$ and t coincide with U and t of our electronic Hamiltonian (3).

APPENDIX B: ET-HgCl CO PHASE: INTERPRETATION OF THE RAMAN SPECTRA IN THE C=C SPECTRAL REGION

The interpretation of the Raman spectra of ET-HgCl in the CO phase is difficult, as many bands crowd in the C=C spectral region. This is particularly evident in the (*bc*) polarized spectrum (top panel of Fig. 12), whereas the parallel polarized spectra (not shown) are dominated a very intense band obscuring the underlying structure.

According the discussion in Sec. III B, the CO pattern is made up of differently charged (+0.4 and +0.6 *e*) ET dimers (Fig 9), and of course the corresponding Raman spectrum cannot be simulated by calculation. The spectral interpretation here is based on a phenomenological approach aimed at reproducing and assigning the experimental frequencies. The frequencies of three C=C stretching (iph-$a_g\nu_2$ and ν_3, oph-$b_{1u}\nu_{27}$) are known to depend linearly from the charge ρ according to [10],

$$\omega_i^{\pm}(\Delta\rho) = \omega_i(0.5) \pm \frac{\Delta\rho \cdot \Delta_i}{2} \qquad \text{(B1)}$$

where the mode frequency $\omega_i^{\pm}$ of the charge rich and charge poor ET dimer is referenced to the experimental frequency at $\rho = 0.5$ (the metallic state), $\Delta\rho$ is the difference between the ionicity ρ of the two dimers in the CO state, and Δ_i is the ionization frequency shift.

Since we are considering the (*bc*) spectrum, we have to take into account that the $\Delta\rho$ dependence of ν_2 and ν_3 is not linear,

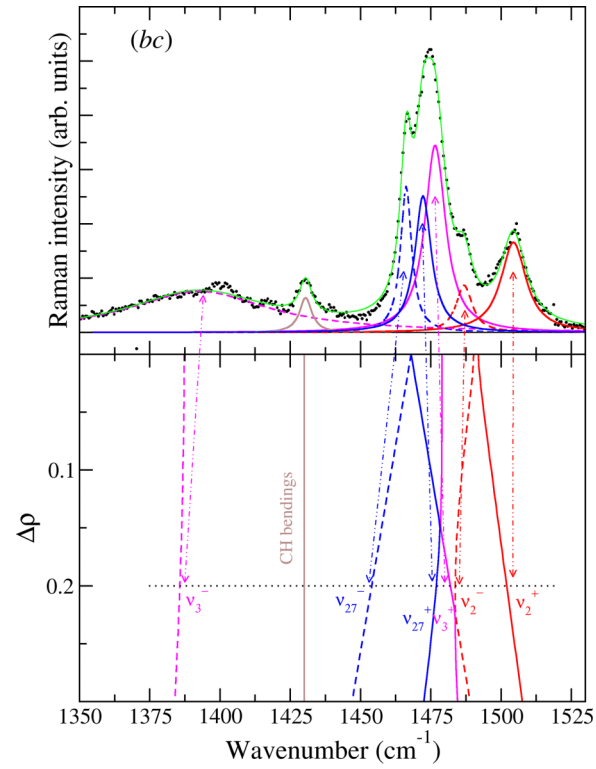

FIG. 12. (Top) Experimental Raman spectrum (*bc* polarization) in the CO phase of ET-HgCl (from Ref. [17]). (Bottom) $\Delta\rho$ dependence of the Raman frequencies, taking into account the effect of interdimer e-mv interaction. The double arrows connecting the two panels indicate the proposed assignment of the bands. The horizontal-dotted line corresponds to the observed $\Delta\rho = 0.2$.

being affected by the interdimer e-mv coupling discussed in Sec. II C. Accordingly, the e-mv perturbed frequencies $\Omega_i^{\pm}$ are obtained from the diagonalization of the following "force constants" matrix

$$F_{ij}^{\pm} = \omega_i^{\pm}\omega_j^{\pm}\delta_{ij} - g_i g_j \chi_R(0)\sqrt{\omega_i^{\pm}\omega_j^{\pm}} \qquad \text{(B2)}$$

where δ_{ij} is the Kronecker delta, $\omega_{i,j}^{\pm}$ and $g_{i,j}$ are the unperturbed frequencies and corresponding e-mv coupling constants [10], and $\chi_R(0)$ the Raman susceptibility.

In the simulation we have added to the three C=C stretching modes just one CH bending in representation of the ones occurring in the spectral region of interest [10]. The frequencies and parameters used in the simulation are reported in Table III. The bottom panel of Fig. 12 shows the results, plotted as the $\Delta\rho$ dependence of the seven $\Omega_i^{\pm}$ frequencies.

TABLE III. Parameters adopted in the phenomenological simulation.

	$\omega_i(0.5)$ (cm^{-1})	Δ_i (cm^{-1})	g_i (meV)
$a_g\nu_2$	1492.0	112.0	30.0
$a_g\nu_3$	1479.0	120.0	71.0
$b_{1u}\nu_{27}$	1468.0	140.0	0.0
CH bend	1447.0	0.0	0.0

All the modes included in the bottom panel of Fig. 12 have the same symmetry. Therefore, the lines expressing their $\Delta\rho$ dependence must obey the noncrossing rule: They approach, but when they become almost degenerate, by perturbation theory they mix and repel each other. Consider first the highest frequency modes, i.e., the red lines corresponding the $a_g\nu_2$ of the charge rich (ν_2^+) and charge poor (ν_2^-) ET molecule. In the $\Delta\rho$ interval considered in the figure, the frequencies have a practically linear dependence [9]. Comparison with the upper panel of Fig. 12 immediately yields the assignment of the ν_2 mode to the band at 1504 cm^{-1} and to the shoulder at 1486 cm^{-1}, as done in Ref. [17]. The estimated $\Delta\rho = 0.2$, evidenced by the horizontal-dotted line, is in agreement with the IR data [18]. Going towards lower frequencies, we have an avoided crossing and quasi-degeneracy between ν_{27}^+ (blue) and ν_3^+ (magenta), and both are assigned to the band seen at 1474 cm^{-1} (we have used two Lorentzians in the deconvolution of the top panel, although one would give an equally good fitting). Proceeding towards lower frequencies we encounter the ν_{27}^-, the CH bending (maroon line) and finally the e-mv perturbed ν_3^-. Therefore, the adopted phenomenological approach gives a satisfactory assignment of the C=C stretching phonons in the CO state of ET-HgCl in terms of two nonequivalent, differently charged dimers.

[1] B. J. Powell and R. H. McKenzie, Quantum frustration in organic mott insulators: From spin liquids to unconventional superconductors, Rep. Prog. Phys. **74**, 056501 (2011).

[2] A. Ardavan, S. Brown, S. Kagoshima, K. Kanoda, K. Kuroki, H. Mori, M. Ogata, S. Uji, and J. Wosnitza, Recent topics of organic superconductors, J. Phys. Soc. Jpn. **81**, 011004 (2012).

[3] J. Wosnitza, Superconductivity in layered organic metals, Crystals **2**, 248 (2012).

[4] M. Dressel and S. Tomić, Molecular quantum materials: Electronic phases and charge dynamics in two-dimensional organic solids, Adv. Phys. **69**, 1 (2020).

[5] K. Riedl, E. Gati, and R. Valentí, Ingredients for generalized models of κ-phase organic charge-transfer salts: A review, Crystals **12**, 1689 (2022).

[6] T. Mori, A. Kobayashi, Y. Sasaki, H. Kobayashi, G. Saito, and H. Inokuchi, The intermolecular interaction of tetrathiafulvalene and Bis(ethylenedithio)tetrathiafulvalene in organic metals. calculation of orbital overlaps and models of energy-band structures, Bull. Chem. Soc. Japan **57**, 627 (1984).

[7] T. Mori, Structural genealogy of BEDT-TTF-based organic conductors. I. Parallel molecules: β and β'' phases, Bull. Chem. Soc. Japan **71**, 2509 (1998).

[8] T. Mori, H. Mori, and S. Tanaka, Structural genealogy of BEDT-TTF-based organic conductors. II. Inclined molecules: θ, α, and κ phases, Bull. Chem. Soc. Jpn. **72**, 179 (1999).

[9] T. Yamamoto, M. Uruichi, K. Yamamoto, K. Yakushi, A. Kawamoto, and H. Taniguchi, Examination of the charge-sensitive vibrational modes in Bis(ethylenedithio)tetrathiafulvalene, J. Phys. Chem. B **109**, 15226 (2005).

[10] A. Girlando, Charge sensitive vibrations and electron-molecular vibration coupling in Bis(ethylenedithio)-tetrathiafulvalene (BEDT-TTF), J. Phys. Chem. C **115**, 19371 (2011).

[11] M. Rice, Towards the experimental determination of the fundamental microscopic parameters of organic ion-radical compounds, Solid State Commun. **31**, 93 (1979).

[12] A. Painelli and A. Girlando, Electron–molecular vibration (e–mv) coupling in charge-transfer compounds and its consequences on the optical spectra: A theoretical framework, J. Chem. Phys. **84**, 5655 (1986).

[13] A. Girlando, M. Masino, S. Kaiser, Y. Sun, N. Drichko, M. Dressel, and H. Mori, Spectroscopic characterization of charge order fluctuations in BEDT-TTF metals and superconductors, Physica Status Solidi Basic Res. **249**, 953 (2012).

[14] A. Girlando, M. Masino, J. A. Schlueter, N. Drichko, S. Kaiser, and M. Dressel, Charge-order fluctuations and superconductivity in two-dimensional organic metals, Phys. Rev. B **89**, 174503 (2014).

[15] M. Maksimuk, K. Yakushi, H. Taniguchi, K. Kanoda, and A. Kawamoto, The C=C stretching vibrations of κ-(BEDT-TTF)$_2$Cu[N(CN)$_2$]Br and its isotope analogues, J. Phys. Soc. Jpn. **70**, 3728 (2001).

[16] T. Yamamoto, T. Naito, M. Uruichi, H. Akutsu, and Y. Nakazawa, Lattice and charge fluctuations in a molecular superconductor, J. Phys. Soc. Jpn. **90**, 063708 (2021).

[17] N. M. Hassan, K. Thirunavukkuarasu, Z. Lu, D. Smirnov, E. I. Zhilyaeva, S. Torunova, R. N. Lyubovskaya, and N. Drichko, Melting of charge order in the low-temperature state of an electronic ferroelectric-like system, npj Quantum Mater. **5**, 15 (2020).

[18] N. Drichko, R. Beyer, E. Rose, M. Dressel, J. A. Schlueter, S. A. Turunova, E. I. Zhilyaeva, and R. N. Lyubovskaya, Metallic state and charge-order metal-insulator transition in the quasi-two-dimensional conductor κ-(BEDT-TTF)$_2$Hg(SCN)$_2$Cl, Phys. Rev. B **89**, 075133 (2014).

[19] A. Löhle, E. Rose, S. Singh, R. Beyer, E. Tafra, T. Ivek, E. I. Zhilyaeva, R. N. Lyubovskaya, and M. Dressel, Pressure dependence of the metal-insulator transition κ-(BEDT-TTF)$_2$Hg(SCN)$_2$Cl: Optical and transport studies, J. Phys.: Condens. Matter **29**, 055601 (2017).

[20] E. Gati, J. K. H. Fischer, P. Lunkenheimer, D. Zielke, S. Köhler, F. Kolb, H.-A. K. von Nidda, S. M. Winter, H. Schubert, J. A. Schlueter, H. O. Jeschke, R. Valentí, and M. Lang, Evidence for electronically driven ferroelectricity in a strongly correlated dimerized BEDT-TTF molecular conductor, Phys. Rev. Lett. **120**, 247601 (2018).

[21] G. Turrell, *Infrared and Raman Spectra of Crystals* (Academic Press, London, 1972).

[22] G. M. J. Barca, C. Bertoni, L. Carrington, D. Datta, N. D. Silva, J. E. Deustua, D. G. Fedorov, J. R. Gour, A. O. Gunina, E. Guidez *et al.*, Recent developments in the general atomic and molecular electronic structure system, J. Chem. Phys. **152**, 154102 (2020).

[23] K. Yakushi, K. Yamamoto, T. Yamamoto, Y. Saito, and A. Kawamoto, Raman spectroscopy study of charge fluctuation in

the spin-liquid candidate κ-(BEDT-TTF)$_2$Cu$_2$(CN)$_3$, J. Phys. Soc. Jpn. **84**, 084711 (2015).

[24] V. M. Yartsev, Electron-molecular vibration coupling in trimerized organic ion-radical semiconductors, Physica Stat. Sol. **112**, 279 (1982).

[25] A. Painelli, C. Pecile, and A. Girlando, Cs_2TCNQ_3 revisited: A detailed description of its ground state through a reinterpretation of the optical spectra, Mol. Cryst. Liq. Cryst. **134**, 1 (1986).

[26] C. Pecile, A. Painelli, and A. Girlando, Studies of organic semiconductors for 40 years—V, Mol. Cryst. Liq. Cryst. Inc. Nonlinear Opt. **171**, 69 (1989).

[27] M. Revelli Beaumont, P. Hemme, Y. Gallais, A. Sacuto, K. Jacob, L. Valade, D. de Caro, C. Faulmann, and M. Cazayous, Possible observation of the signature of the bad metal phase and its crossover to a Fermi liquid in $\kappa-$(BEDT-TTF)$_2$Cu(NCS)$_2$ bulk and nanoparticles by raman scattering, J. Phys.: Condens. Matter **33**, 125403 (2021).

[28] M. Tamura, H. Tajima, K. Yakushi, H. Kuroda, A. Kobayashi, R. Kato, and H. Kobayashi, Reflectance spectra of κ-(BEDT-TTF)$_2$I$_3$: Electronic structure of dimeric BEDT-TTF salts, J. Phys. Soc. Jpn. **60**, 3861 (1991).

[29] H. Kino and H. Fukuyama, Electronic states of conducting organic κ-(BEDT-TTF)$_2$X, J. Phys. Soc. Jpn. **64**, 2726 (1995).

[30] R. H. McKenzie, A strongly correlated electron model for the layered organic superconductors κ-(BEDT-TTF)$_2$X, Comments Cond. Matt. Phys. **18**, 309 (1998). See also arXiv:cond-mat/9802198.

[31] K. Sedlmeier, S. Elsässer, D. Neubauer, R. Beyer, D. Wu, T. Ivek, S. Tomić, J. A. Schlueter, and M. Dressel, Absence of charge order in the dimerized κ-phase BEDT-TTF salts, Phys. Rev. B **86**, 245103 (2012).

[32] A. Pustogow, Thirty-year anniversary of κ-(BEDT-TTF)$_2$ Cu$_2$(CN)$_3$: Reconciling the spin gap in a spin-liquid candidate, Solids **3**, 93 (2022).

[33] P. Foury-Leylekian, V. Ilakovac, V. Balédent, P. Fertey, A. Arakcheeva, O. Milat, D. Petermann, G. Guillier, K. Miyagawa, K. Kanoda *et al.*, (BEDT-TTF)$_2$Cu$_2$(CN)$_3$ spin liquid: Beyond the average structure, Crystals **8**, 158 (2018).

[34] J. Liebman, K. Miyagawa, K. Kanoda, and N. Drichko, Novel dipole-lattice coupling in the quantum-spin-liquid material κ-(BEDT-TTF)$_2$Cu$_2$(CN)$_3$, arXiv:2403.02676.

[35] K. Suzuki, K. Yamamoto, and K. Yakushi, Charge-ordering transition in orthorhombic and monoclinic single-crystals of θ-(BEDT-TTF)$_2$TlZn(SCN)$_4$ studied by vibrational spectroscopy, Phys. Rev. B **69**, 085114 (2004).